CHARACTERIZATIONS OF MARTIAN WATER-ICE CLOUD CRYSTAL GEOMETRIES FROM PHASE FUNCTIONS DERIVED USING MARCI IMAGE DATA

B. A. Cooper, R. Modestino , C. L. Smith, J. E. Moores
Centre for Research in Earth and Space Science, York University, 4700 Keele St. Toronto, ON, Canada, M3J 1P3

Figure (1):

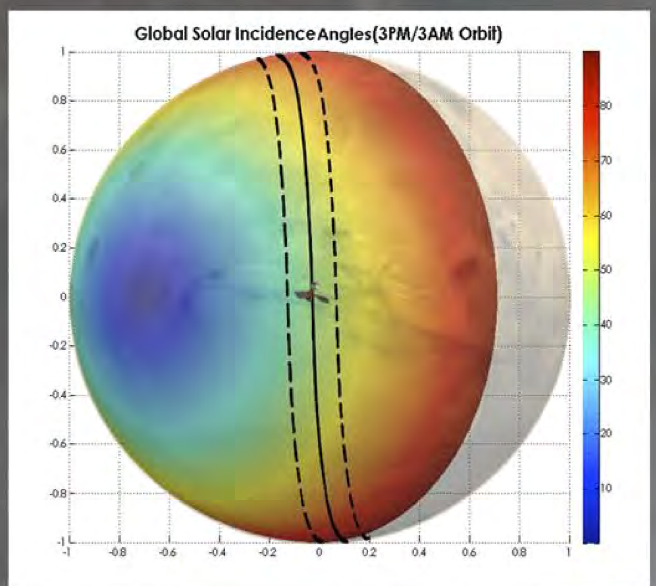

Figure (2):

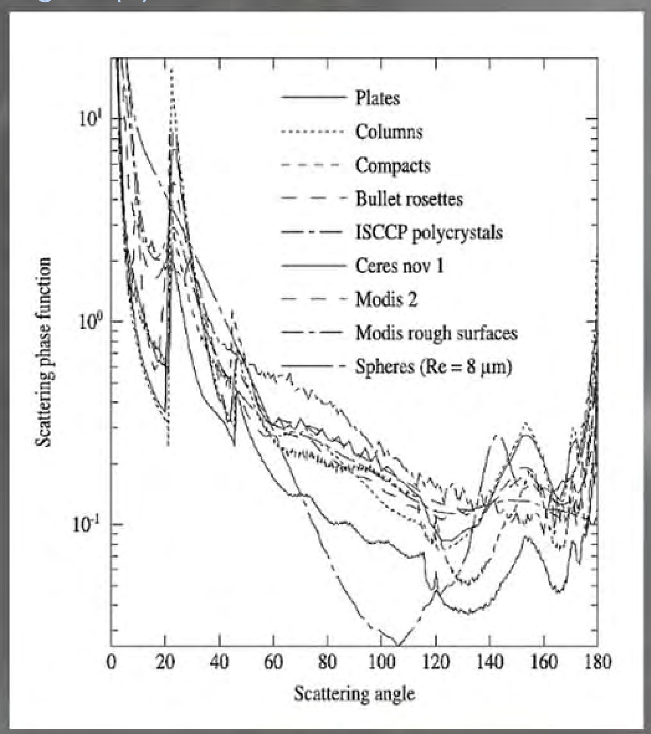

Introduction

The Mars Color Imager (MARCI) was launched aboard the Mars Reconnaissance Orbiter (MRO) in early August of 2005. During the orbiter's primary science phase (PSP), MRO was locked in a 3am-3pm sun-synchronous orbit (as seen in *Figure (1)* with approximate orbit and swath), allowing MARCI to capture 12 to 13 images per Martian day in 5 visible and 2 ultraviolet wavelengths. These filters were permanently mounted on top of MARCI's 180° field of view (FOV) charge coupled device (CCD), operating as a 'pushbroom' imager capturing frames every few seconds.

Our work seeks to derive the phase function of Martian water-ice clouds through the analysis of MARCI images taken during the PSP. We will then use the phase function data to deduce the dominant geometries of water-ice crystals in Martian clouds by comparing the phase functions to their corresponding scattering angles over the course of the entire PSP.

Figure (2) displays a plot from Chepfer et al., 2002 of 14 different ice crystal scattering angles retieved in a laboratory setting that we will use as a step-stone for this comparison.

We take into account the angles at which the clouds were observed by MARCI and the angles at which they received incident solar radiation, to have a thorough understanding of how the ice crystals in any image pixel scatter light.

MARCI Instument

MARCI utilizes a 1024 × 1024 pixel CCD with seven narrowband interference filters bonded directly to its surface. Every 'framelet' on the VIS and UV CCD is comprised of 16 pixel rows downtrack with a 2° degree FOV and 1024 pixel colums cross-track with a 180° FOV. The five filter framelets are combined to make a single frame with dimensions of 80 x 1024 pixels for the visual and the two for the UV produce a 32x1024 frame.

Visual Bands					
Band:	1	2	3	4	5
Filter Name:	420 nm	550 nm	600 nm	650 nm	720 nm
λ_{eff} (nm)	437.2	546.3	604.2	653.1	717.7
Ultraviolet Bands					
Band:	1		2		
Filter Name:	260 nm		320 nm		
λ_{eff} (nm)	258.1		319.9		

Figure (3): Table depicting VIS & UV Bands at which MARCI observes (Data from Bell et al., 2009)

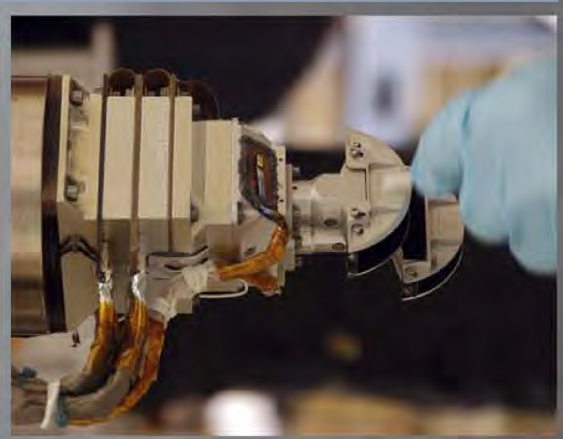

Figure (4): MARCI (image: MSSS)

Figure 5 (a)

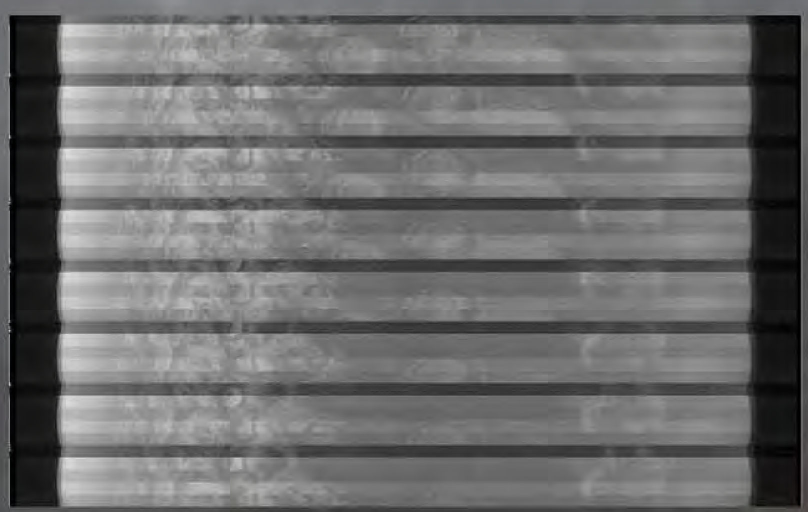

Figure 5 (b)

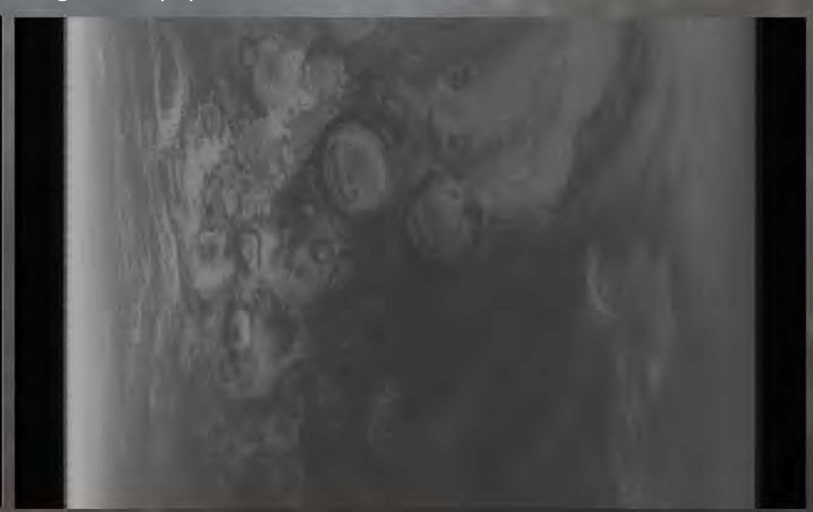

Figure 5: (a) displays part of a calibrated MARCI image with each frame in the image strip consisting of 5 different VIS filter framelets. In order to work with the images, we had to divide each MARCI image into 5 separate images, one for each filter. (b) displays the same region as (a), but consisting of only the red filter framelets which were isolated and concatinated to produce a much more cohesive image in only that particular wavelength.

Radiometric Calibration

The MARCI PSP data used in this work was obtained from the Planetary Data System and was radiometrically calibrated in accordance with the calibration documents published by Bell et al., 2009. The pixel values of the raw images were converted into units of spectral radiance, and from there reflectance values were derived by dividing the spectral radiance by the solar flux Mars received at the time of image capture.

For greater accuracy, the radiative flux for each image was calculated based upon Mars' distance from the Sun, which is dictated by the planet's position in its orbit. This parameter, also known as 'solar longitude', was calculated using the spacecraft clock time found in each image's header, in an adaptation of the NASA Mars24 algorithm that we produced for MARCI.

Phase Function Calculation

The phase function is defined as the angular distribution of light intensity scattered by a particle at a given wavelength, and it is directly dependent upon the angle between the incident radiation and the scattered radiation detected, known as the 'scattering angle'.

We produced a matrix of viewing geometries from the orbiter, corresponding to every photoactive pixel on the MARCI CCD, along with a matrix of incident radiation angles based upon MRO's orbit in the PSP. These angle matrices were used in conjunction with the calibrated reflectance data for each filter, along with Martian atmospheric parameters, as inputs for an adapted equation from Wang et al., 2014 to compute phase functions.

As a result of MARCI's orbital vantage point, a majority of the reflectance data in each image comes from the Martian surface. In order to isolate the pixels containing clouds, we cropped our calculation range to exclude the polar caps and the atmospheric limbs, and then made the assumption that the pixels with the highest reflectance values in all visible filters would be those belonging to clouds. This is a safe assumption as water-ice clouds scatter uniformly through all visible wavelengths andhave much higher albedos than Martian equatorial regions.

Method / Analysis

We created a pipeline which calibrated, separated, cropped, and reduced images, as well as calculated and output reflectance, spectral radiance and phase function values. We ran through the thousands of images captured during the PSP with our program for both visual and ultraviolet filters, logging the output data on each run. The plots below show the outputs from our first run through of the PSP, displaying the phase function with respect to scattering angle and solar longitude, as well as blue and red filter ratios to better understand how much of the atmospheric phase function comes from dust versus clouds. These outputs have led us to notice a number of interesting features, some which can be immediately deemed artificats, some which are the result of approximations that we hope to adjust in a future run, and some that we will work to show are real, in our next steps.

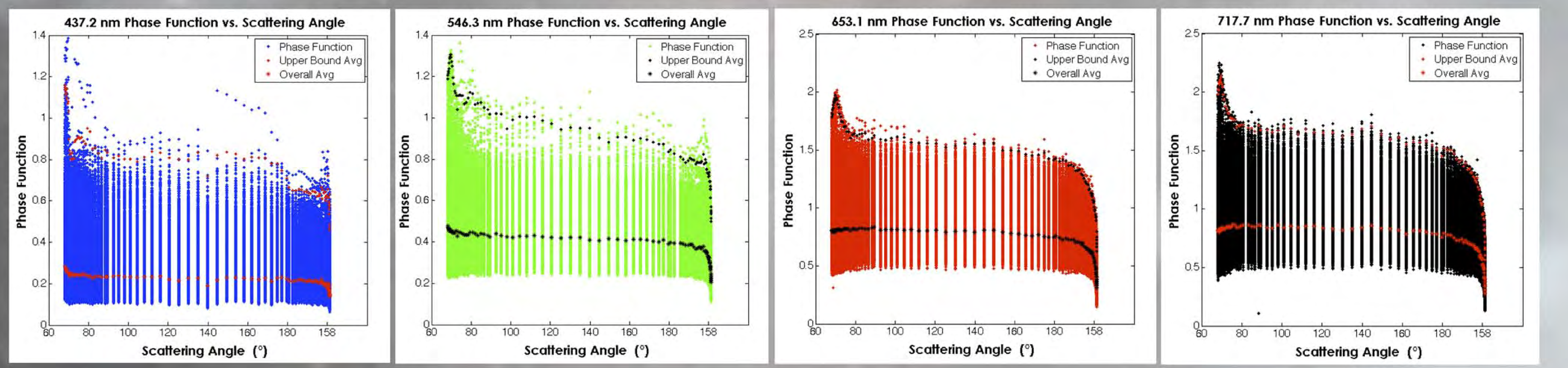

Figure 6 (Above): Phase function plots for 4/5 visual filters. Right away we notice that we have not fully accounted for the solar flux varying across the image.

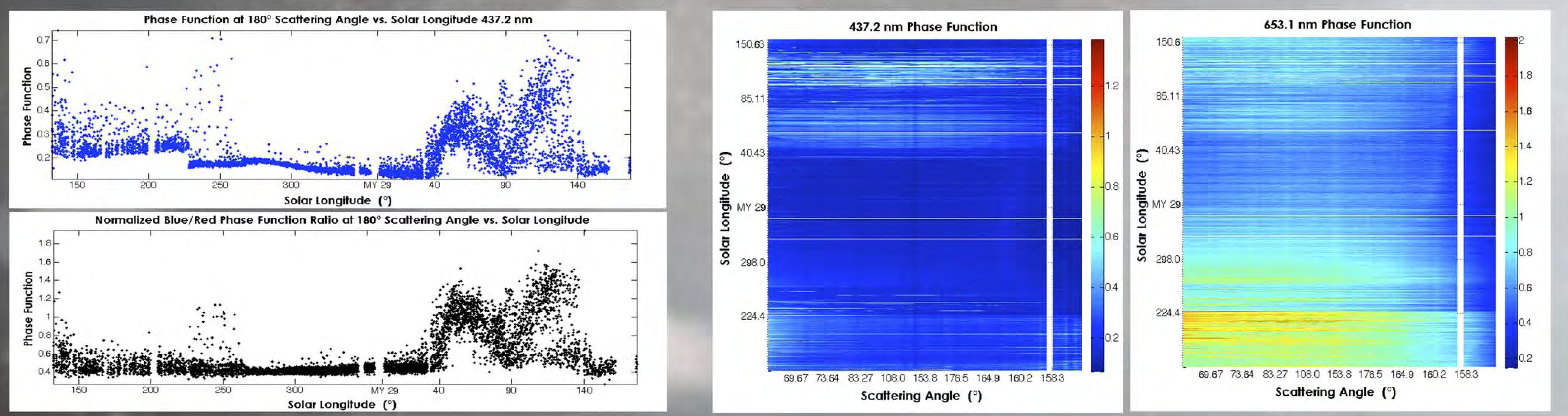

Figure 7 (Above): Phase Function over the course of the PSP in both red and blue filters are displayed in surface plots, while just the blue filter and the B/R ratio are displayed in scatter plots. Notice the discontinuous drop around Ls=225. It was discovered after our run that after this date the exposure times varied within each image and that data was kept in a separate file outside of the image header. For the B/R plot, any values >1 show phase function contributions from mostly clouds, as opposed to dust.

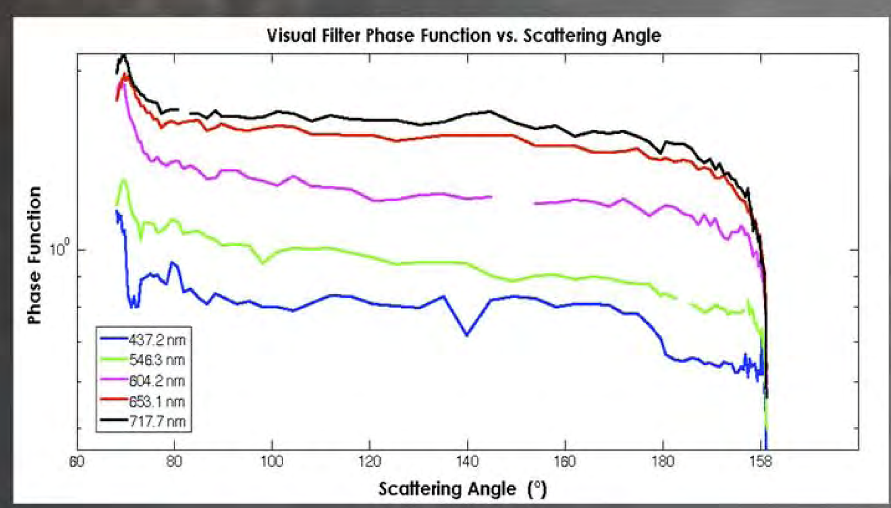

Figure 8: Averaged upper boundary of each visual filter.

Next Steps

From the data output so far, we note that this is very much still a work in progress. We need to account for the flux variation over the image frame which appears to be overpowering most phase-function features, including the 180 degree back scatter surge, which we'd expect at the very least. Additionally, when the extra data files mentioned in the *Figure 6* caption were found, a number of values our program was calculating or approximating were found explicitly given, and so it will be interesting to not only compare, but update the pipeline with these more accurate input parameters as well. Once the updated program is completed, we will run through the PSP images again, and begin our comparison of phase-function plots to try to constrain the dominant geometries of the ice crystals which make up Martian water-ice clouds. We also hope to investigate how the phase function varies seasonally, as well as get a deeper look at the phase-function contributions from dust versus clouds.

References

Allison, M., and M. McEwen. "A post-Pathfinder evaluation of aerocentric solar coordinates with improved timing recipes for Mars seasonal/diurnal climate studies". Planet. Space Sci. 48, 215-235 2000).

Bell, J. F., et al, "Mars Reconnaissance Orbiter Mars Color Imager (MARCI): Instrument descripti(on, calibration, and performance." Journal of Geophysical Research 114, no. E8 (2009).

Chepfer, Helene ,et al. "Estimation of cirrus cloud effective ice crystal shapes using visible reflectances from dual-satellite measurements." Journal of Geophysical Research: Atmospheres 107, no. D23 (2002).

Wang, Chenxi, et al. "Estimation of the cirrus cloud scattering phase function from satellite observations." Journal of Quantitative Spectroscopy and Radiative Transfer 138 (2014): 36-49.